INTERNATIONAL JOURNAL OF PHARMACEUTICAL SCIENCES
[ISSN: 0975-4725; CODEN(USA): IJPS00]
Journal Homepage: https://www.ijpsjournal.com

OPEN ACCESS

Research Paper

In-silico Prediction, Fabrication, Characterization and Wound Healing Activity of Polymeric Based Curcumin-Nimbin Loaded Nanosuspension for Diabetic Foot Ulcer Using Diabetogenic Induced Rat Models

Gnana Prakash Victor*[1], Senthil Kumar Chinnamaruthu[2], Nithyasri Jayavel[3], Mohamed Nizar Mustafa[4], Eraiarasu Mahadevan[5], Mohan Sellappan[6]

[1] Department of Pharmaceutical Analysis, National Institute of Pharmaceutical Education and Research - Ahmedabad (NIPER-A), Opposite Air Force Station, Palaj, Gandhinagar, Gujarat, India – 382355.
[2] Department of Pharmacology, RVS College of Pharmaceutical Sciences, Sulur, Coimbatore, Tamilnadu, India; INTI International University, Malaysia.
[3] Department of Pharmaceutics, Krupanidhi college of pharmacy, Bengaluru, India.
[4,5] Karpagam College of Pharmacy, Coimbatore, Tamilnadu, India.
[6] Department of Pharmaceutics, Coimbatore College of Pharmacy, Karumathampatti, Coimbatore, Tamilnadu, India..

ARTICLE INFO

Published: 30 June 2026
Keywords:
Curcumin, Nimbin, Diperoxochloric acid, Diabetic foot ulcer, in silico docking..
DOI:
10.5281/zenodo.21066238

ABSTRACT

This study aims to fabricate, characterize and evaluate the wound healing activity of a polymeric based dual-loaded nanosuspension containing Curcumin (CUR) and Nimbin (NIM) to enhance diabetic foot ulcer (DFU) healing. An In-silico approach was employed to predict the binding capacity of CUR and NIM with wound healing targets (TIMMPs, MMP-8, IL-1, IL-6, IL-20, IL-22, IL-24, and MMP-9) using molecular docking and ADMET profiling. NIM was isolated from Azadirachta indica seed extract and subjected to phytochemical screening. The polymeric based CUR-NIM loaded nanosuspension was prepared through sonication based on nanoprecipitation method using β-cyclodextrin (β-CD) as polymer and sodium lauryl sulphate (SLS) as surfactant and characterized for mean particle size, Polydispersity Index (PDI), Zeta potential, UV-Visible spectral and FTIR analysis. In-vivo studies were performed using streptozotocin-induced diabetic rat models compared to the positive control (Diperoxochloric acid). In-silico studies confirmed significant binding affinity of CUR with MMP-9, IL-20 and NIM with MMP-8, IL-20, supporting their synergistic wound healing activity comparatively standard drug. The nanosuspension was attributed to

***Corresponding Author:** Gnana Prakash Victor
Address: *Department of Pharmaceutical Analysis, National Institute of Pharmaceutical Education and Research - Ahmedabad (NIPER-A), Opposite Air Force Station, Palaj, Gandhinagar, Gujarat, India – 382355.*
Email ✉: gnanaprakashv28@gmail.com
Relevant conflicts of interest/financial disclosures: The authors declare that the research was conducted in the absence of any commercial or financial relationships that could be construed as a potential conflict of interest.

particle size reduction which enhanced solubility, permeability and CUR reactivity through its incorporation with NIM. DLS analysis showed CUR-NIM nanoparticles (Z-average size ~380.6 nm, size distribution by volume ~100nm, PDI 0.5421, Zeta potential -26 mV) with moderate stability, absence of aggregation, acceptable heterogeneity and suitable size for topical delivery. In-vivo studies showed significantly equivalent wound contraction, epithelialization rate and collagen deposition in treated groups compared to the positive control ($p < 0.05$). Overall, the formulation demonstrated remarkable wound healing efficiency, underscoring its potential as a promising therapeutic strategy for DFU

INTRODUCTION

According to the World Health Organization (WHO), around 422 million people currently live with diabetes mellitus (DM) and this number is expected to increase by approximately 271 million by the year 2045[1]. In pharma market, many medications and treatments are available to treat diabetes so far have only been able to manage blood glucose levels; they do not yet have the ability to fully cure the condition. Diabetes mellitus may lead to chronic complications as the results of improper control such as cardiovascular diseases, diabetic nephropathy (kidney diseases), ischemia (inadequate blood flow), diabetic neuropathy (nerve damages), diabetic retinopathy (eye damages), diabetic foot ulcers and others like skin problems, hearing loss, dementia including Alzheimer's disease[2].

Diabetic foot ulcer (DFU) is biggest public health issues the world has ever faced in people with uncontrolled diabetes. Neuropathy caused by hyperglycemia which may develop the DFU. The hyperglycemic state enhances the activity of the enzymes such as sorbitol dehydrogenase and aldose reductase, which converts the intracellular glucose to fructose and sorbitol. Myoinositol production in nerve cells is reduced as a result of the buildup of converted glucose products. Nicotinamide adenine dinucleotide phosphate (NADP), which is necessary for the detoxification of reactive oxygen species (ROS) and the creation of the vasodilator nitric oxide (NO), is also depleted as a result of the chemical alteration linked to glucose. Following this, there is an increase in oxidative stress on the nerve cells and vasoconstriction that results in ischemia, which damages and kills the nerve cells. The sensory, motor and autonomic nerve systems are all impacted by neuropathy. The sebaceous and sweat glands secretory capabilities are diminished in autonomic neuropathy, the foot becomes dry and is unable to moisten its surface, which promotes the spread of infections[3][4].

Globally, chronic foot ulcers are estimated to affect 6.3% of individuals with diabetes (95% CI: 5.4 to 7.3%), with men experiencing a higher prevalence than women [2]. From 2003 to 2017, the incidence of newly diagnosed diabetic foot ulcers (DFU) rose markedly, increasing from 20.7 to 33.1 cases per 1,000 patients ($P < 0.0001$)[5]. The occurrence of DFU varies considerably across regions, but it is projected that up to one-quarter of diabetic patients may develop foot ulcers during their lifetime. These ulcers represent a major risk factor for lower extremity amputation (LEA), involving the feet and legs[6]. The International Diabetes Federation (IDF) highlights that individuals with diabetes face a 10–30 times greater likelihood of amputation compared to non-diabetic populations. Overall, 15–25% of diabetic patients are affected by DFU, and both DFU and subsequent amputations remain leading contributors to morbidity and mortality. Notably, approximately 85% of amputations in diabetic patients are preceded by DFU, which often progresses to severe infection or gangrene[2].

Current marketed topical drugs used for DFU such as Diperoxochloric acid, Cadexomer iodine, Luliconazole cream, Povidone iodine, Mupirocin, Becaplermin, Sertaconazole nitrate and Clotrimazole. Inspite of all the therapeutic value it has many side effects such as allergic reaction like

rash, hives, itching; red, swollen, blistered, or peeling skin with or without fever, swelling of face, lips, tongue, or throat[7][8][9][10]. In order to minimize the above side effects, we planned to formulate herbal based treatment which could be used for controlling the diabetic foot ulcer. Herbal remedies have been trusted for managing health conditions since ancient times. Modern scientific investigations highlight that medicinal plants contain bioactive compounds with diverse pharmacological effects, capable of protecting cells from harmful damage, including those seen in chronic diabetic wounds. Evidence suggests that using these medicinal plants and their active constituents can help lessen the complications associated with diabetic foot ulcers (DFUs)[11][12].

Plant-derived compounds such as curcumin and nimbin exhibit a wide range of therapeutic properties, including anti-inflammatory, antipyretic, fungicidal, antihistaminic, and antiseptic effects. These bioactive molecules have been shown to play a role in managing oxidative stress and inflammatory disorders, as well as conditions like metabolic syndrome, arthritis, anxiety, and hyperlipidaemia. Additionally, they may contribute to alleviating exercise-induced inflammation and muscle soreness, thereby supporting recovery and improving performance in physically active individuals.

Curcumin, a biologically active compound obtained from the dried rhizomes of Curcuma longa, is renowned for its diverse health-promoting effects, particularly its role in supporting wound healing. But its therapeutic effectiveness is limited due to poor water solubility and low stability in aqueous environments. Neem seed kernels have a lot of Phyto-isolates like Azadirachtin and the others are nimbolinin, nimbin, nimbidin, nimbidol, sodium nimbinate, gedunin, salannin and quercetin. Among those, the biologically active compound is Nimbin which is a promising candidate to promote the wound healing and also act as a synergistic molecule to enhance the anti-inflammatory activity of Curcumin with the help of dual-loading approach to treat the DFU[13][14][15][16][17][18][19]. Though many herbal based Phyto-active compounds in different formulations are available in the treatment of diabetic wound healing, but it has several limitations are low absorption, low permeability, no site specific, low bioavailability & efficacy, high toxicity, limited knowledge regarding its underlying pathogenesis and failure to remodeling & regenerate the skin by various wound healing biomarkers (Down regulation of Tissue inhibitors of metalloproteinases (TIMMPs), Matrix metalloproteinase-8 (MMP-8) and up-regulation of Interleukins (ILs) such as IL-1, IL-6, IL-20, IL-22, IL-24 and MMP-9.

To overcome these limitations, we performed *In-silico* evaluations such as Drug likeness (Molinspiration), ADMET prediction (pkCSM software) and Molecular docking (PyRx Software, PyMOL Application, BIOVIA Discovery Studio Visualizer) to systematically determine the significant binding affinity of ligands with the respective biomarkers of DFU and hypothesized a novel drug delivery system such as polymeric based Nano-formulation by using nano-precipitation method. Nanoparticles (NPs) promote the wound healing activity by improving the characteristics of surface area to volume ratio, porosity, solubility & permeability through reducing the particles size. They also improve the encapsulation of bioactive compounds, enabling controlled release and facilitating active cellular interactions with the polymeric matrix during functionalization and tissue remodelling. Formulations of polymeric NPs loaded with curcumin and nimbin have demonstrated increased collagen deposition in treated wounds, thereby accelerating the healing process.

MATERIALS AND METHODS

Materials

The following online tools/offline software's such as PubChem for retrieving the 2D- and 3D-structure of the ligands, RCSB database for curated collection of 3D structure of proteins, pkCSM for evaluating the drug-likeness properties, SwissADME for pharmacokinetics (ADMET) prediction, SPDB viewer for target protein preparation, BIOVIA Discovery studio for ligand collection and clustering, PyRx for conducting *In-silico* docking, PyMOL for building the protein-ligand complexes.

The seeds of Azadirachta indica were collected from the campus of Karpagam College of Pharmacy, Coimbatore. They were authenticated by Botanical Survey of India, Southern Regional Centre, T.N.A.U Campus, Coimbatore with the authentication number of Azadirachta indica BSI/SRC/5/23/2022/Tech/649 and the Curcumin (5g) was purchased from Sigma Aldrich, Bangalore with the product number C1386 and CAS-No: 458-37-7. β-cyclodextrin (β-CD), Sodium lauryl sulphate (SLS), Diperoxochloric acid topical solution (WOXheal), Streptozotocin, Ketamine Hydrochloride, Methanol were purchased and Instrumentation's like Rotary evaporator, Ultra-sonicator (Bath sonicator), UV-Visible spectrophotometer (Shimadzu UV-1800), Fourier transform infrared (FT-IR) spectroscopy, Malvern zeta sizer, pH meter was used.

Healthy adult of either sex Albino Wistar rats weighing between 150 – 200 gm were obtained from the animal house of Karpagam Academy of Higher Education, Coimbatore, Tamil Nadu. Animals were cared in compliance with the "Guide for the Care and Use of Laboratory Animals" (NIH, 1985), and all experimental procedures were carried out in accordance with the regulations of the "Committee for the Purpose of Control and Supervision of Experiments on Animals" (CPCSEA). The pharmacology and acute toxicity protocols were approved by Institutional Animal Ethics Committee with KAHE/IAEC/2023/04-02/014.

In-silico prediction

Drug likeness (or) Lipinski rule of five

Lipinski's rule of five (Ro5) is the key to evaluate drug-likeness, it helps to whether the chemical compound with particular pharmacological or biological activity has the correct chemical and physical properties that would make it an orally active therapeutic compound in humans. Drug-likeness describes the ability of a molecule to undergo absorption, achieve bioavailability, and distribute effectively through the intestinal system. To evaluate drug similarity, the rule of five considers parameters including hydrophobicity, electronic features, hydrogen bonding, molecular dimensions, flexibility, and pharmacophoric traits. These factors govern the molecule's performance in living organisms, influencing absorption, distribution, protein affinity, reactivity, toxicity, metabolic stability, and more. Therefore, the Molinspiration online platform was employed to evaluate the drug-likeness of the chosen ligand molecules. The Rule of Five (Ro5) is based on five key physicochemical thresholds: molecular weight (MW) should be below 500 Daltons, lipophilicity (LogP) under 5, hydrogen bond donors fewer than 5, hydrogen bond acceptors fewer than 10, and a Topological Polar Surface Area (TPSA) less than 140 $Å^2$. Ligands that fail to meet these criteria are likely to present difficulties when administered orally. Moreover, if a compound violates two or more of these parameters, it is generally classified as unsuitable for oral drug availability[20][21].

ADMET prediction of ligands

ADMET profiling of the ligands was carried out using pkCSM and SwissADME tools. This online platform can predict the various pharmacokinetics

and pharmacology for absorption, distribution, metabolism and excretion along with forecasting possible toxicity profiles of the molecules under investigation. The respective parameters of dermally applied products are aqueous solubility, skin permeation, AMES toxicity and skin sensitization were predicted[22].

Docking interaction analysis

The three-dimensional (3D-) and two-dimensional structure (2D-) of the ligands such as Curcumin (CUR), Nimbin (NIM), selected Standard drug Diperoxochloric acid (DPOCL) was obtained from the PubChem database **(Figure 1)** in (.sdf) format and converted into (.pdb). Then, clustering the ligands and save it as (.mol) using BIOVIA Discovery studio Visualizer. Additionally, canonical SMILES were obtained from the PubChem database. The molecular structure is described by canonical SMILES as a graph with optional chiral indicators. Protein structures in 3D form were downloaded from the RCSB Protein Data Bank (PDB) using Spdb viewer. The chosen drug targets Interleukins (IL-1, IL-6, IL-20, IL-22, IL-24), Matrix Metalloproteinases (MMP-8, MMP-9), and TIMPs are biomarkers involved in signalling and metabolic pathways relevant to disease mechanisms. These proteins were collected by using PDB id and the role of the above targeted proteins in Diabetic foot ulcers (DFUs) compared with Diabetic mellitus (DMs) which are listed in the **(Table 1)**[23][24]. Firstly, remove the selected unwanted amino acids, water molecules and other residues from the obtained proteins. For docking process using PyRx software. Here, the energy of ligand molecules was minimized and the ligand molecules that had their energy minimised were then converted into Auto Dock ligand in the (. pdbqt) format. Proteins were covered by an appropriate grid box after importing the macromolecules. After the docking process completed, the binding affinity of all the selected ligands with suitable proteins/biomarkers was predicted. Save the file extension in (.csv) format. Building the Protein ligand complex using PyMOL application and save it as protein-ligand complex (.pdb) format. To Study Protein-Ligand interactions, BIOVIA discovery studio visualizer was used that it shows binding sites, receptor cavities, 2D & 3D binding sites, Ramachandran plot, Hydrophobicity visualization, Contact mapping, Hydrogen-bond interaction plot[25][26][27].

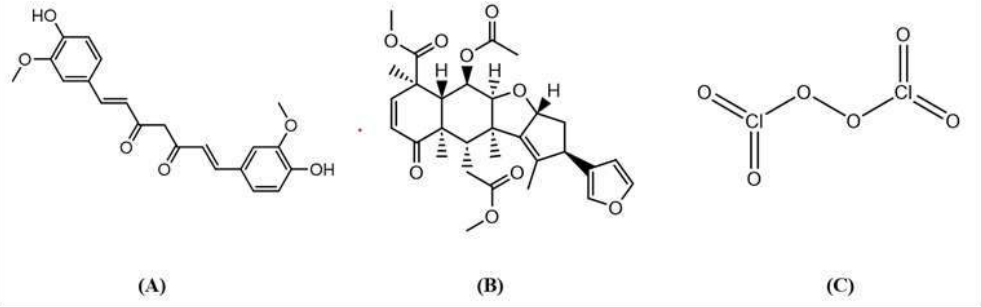

Figure 1: Chemical structures; **(A) CURCUMIN - PUBCHEM CID: 969516** ((1E,6E)-1,7-bis(4-hydroxy-3-methoxyphenyl) hepta-1,6-diene-3,5-dione); **(B) NIMBIN – PUBCHEM CID: 108058** (methyl(1S,2R,3R,4R,8R,9S,10R,13R,15R)-2-acetyloxy-13-(furan-3-yl)-9-(2-methoxy-2-oxoethyl)-4,8,10,12-tetramethyl-7-oxo-16-oxatetracyclo [8.6.0.03,8.011,15] hexadeca-5,11-diene-4-carboxylate); **(C) DIPEROXOCHLORIC ACID - PUBCHEM CID: 135390789** (chloryloxy chlorate)

Table 1: Targeted proteins for molecular docking & its role in Diabetic foot ulcer (DFUs)

S. No	Targets (Proteins)	PDB ID	Changes in DFU (compared with DMs)	Role in DFUs
1.	Interleukin-1 (IL-1)	1ILR	Up regulating (↑)	Regulating immunity and compare to IL-1 that the IL-6 is a suitable candidate biomarker for the determination of the disease progression of DFU.
2.	Interleukin-6 (IL-6)	1ALU		
3.	Interleukin-20 (IL-20)	4DOH	Up regulating (↑)	Promoting wound repair in DM by improving keratinocyte pro-healing functions and they can provide therapeutic benefit for DFU patients by accelerating the healing process of DFU.
4.	Interleukin-22 (IL-22)	1M4R		
5.	Interleukin-24 (IL-24)	6GG1		
6.	Matrix metalloproteinase-8 (MMP-8)	1L6J	Down regulating (↓)	MMP-8 is a non-competitive inhibitor and MMP-9 playing an important role in collagen degradation and tissue destruction. These are the suitable candidate for delayed healing.
7.	Matrix metalloproteinase-9 (MMP-9)	1A86	Up regulating (↑)	
8.	Tissue inhibitors of metalloproteinase (TIMP)	1BR9	Down regulating (↓)	Plays an important role in delayed wound healing.

Extraction and Isolation of Nimbin (NIM)

From 1kg of mature neem seeds, the seed coats were crushed and removed, yielding 300g of kernels. These kernels were ground into powder and defatted with hexane (500ml × 3) over 12h. The defatted kernels were subsequently extracted with 1.5L methanol around 12h using a mechanical stirrer. The resulting extract was filtered and concentrated under reduced pressure with a rotary evaporator, producing approximately 70g of crude extract. The ethyl acetate (EtOAc) layer was separated and concentrated after partitioning with EtOAc (100ml x 3 times) and water to get 30g of final crude. Additionally, this was subjected to repeated silica gel column chromatography (100 to 120 mesh) with a hexane and EtOAc solvent system. Around 70:30 (Hexanes: EtOAc), the required NIM eluted, yielding 600mg of NIM[28].

Preliminary phytochemical screening of Neem seed extract and NIM

Preliminary phytochemical screening was carried out on the seed extract of Azadirachta indica along with the isolated compound NIM. The analysis aimed to detect phytoconstituents such as alkaloids, flavonoids, saponins, glycosides, polyphenols, tannins, steroids and coumarins, while specifically confirming terpenoids in NIM recognized for their wound-healing potential. The screening was performed following standard procedures reported in the literature **(Table 2)**[29][30][31].

Table 2: Procedure for Phytochemical screening of Neem seeds & Nimbin

S. No	Phytochemicals	Name of test	Procedure	Colour indication for presence
1.	Alkaloids	Mayer's test	Extract was treated with Mayer's reagent.	Green colour precipitate
		Wagner's test	Extract was treated with Wagner's reagent.	Brick colour
2.	Flavonoids	Alkaline reagent test	Extracts were treated with few drops of NaOH solution.	White intense yellow colour, which becomes colourless on addition of dilute acid.
		Shinoda test	Extract was treated with few drops of Hydrochloric acid and 0.5 gm of magnesium pieces.	Pink colour
3.	Saponins	Foam test	Extract solution was diluted with distilled water.	Suspension formed for minutes. Two cm layer of foam.
4.	Glycosides	Salkowski's test	Extract was treated with chloroform. Then 2ml of concentrated H_2SO_4 was added and shaken gently	Reddish brown colour
		Keller-killani test	Extract was treated with glacial acetic acid containing 1-2 drops of 2% solution of $Fecl_3$. The mixture was poured into another test tube containing 2ml of concentrated H_2SO_4.	Brown ring at the interface.
5.	Terpenoids	Terpenoids test	Extract was dissolved in chloroform and evaporated to dryness. To this concentrated H_2SO_4 was added.	Reddish brown colour at the interface
6.	Polyphenols and tannins	Polyphenols and Tannins	Extract was mixed with 2% solution of $Fecl_3$.	Blue green or blue-black colour
7.	Steroids	Steroids test	Extract was treated with chloroform and concentrated H_2SO_4 was added sidewise.	Red colour produced in the lower chloroform layer
8.	Coumarins	Coumarins test	Extract solution is concentrated to yield a residue. Dissolve residue in hot water. After cooling divide solution in two test tubes. To one test tube add 10% (w/v) Ammonium Hydroxide. Other test tube was used as control.	Fluorescence colour

Fabrication of Polymeric based CUR-NIM loaded nanosuspension

A polymeric based CUR-NIM loaded nanosuspension was formulated through the nanoprecipitation technique under ultrasonic treatment. In brief, 25mg of curcumin (CUR) and 25mg of nimbin (NIM) were dissolved in 20mL of methanol. This organic solution was rapidly introduced into 50mL of distilled water containing varying concentrations of sodium lauryl sulfate (SLS) and β-cyclodextrin (β-CD), while sonication was applied at 40 kHz (Lark, India). However, to ensure complete removal of residual methanol, the sonication process was extended for an additional hour. The resulting nanosuspension was subjected to centrifugation (Remi, India) at 19,000 rpm for 45 minutes at -20°C to collect the CUR-NIM nanoparticles stabilized with SLS/β-CD. Then, the pellet was washed to remove impurities and re-dispersed it in distilled water to get a purified nanosuspension. Finally, particle size distribution, polydispersity index (PDI) and zeta potential of the nanosuspension were determined using a Mastersizer instrument (Malvern, UK)[15][16].

Characterization of Polymeric based CUR-NIM loaded nanosuspension

The prepared nanosuspension was subjected to morphological, physical, and chemical characterization using a different analytical technique, including UV-Visible spectroscopy, FTIR analysis and particle size/zeta potential measurements with a Malvern Zetasizer[16][32][33][34][35].

UV-Visible spectral analysis

The prepared polymeric based CUR-NIM loaded nanosuspension's optical property was monitored using the UV-Visible spectroscopy. 1ml of the mixture was sampled periodically (every half an hour) and their spectrums were measured with a UV-Visible spectrophotometer (Shimadzu, UV 2500) in the range of 200nm to 800nm. It is a valuable method for the characterization of the absorbance bands of nanoparticles especially metals because they are intensely colored and show absorptions due to surface plasmon oscillations. Light waves that interact with the metal's free electrons and become trapped on the surface are known as surface plasmons.

Fourier transforms infrared spectroscopic (FTIR) analysis

The functional groups involved in the formation of nanoparticles within the nanosuspension were analyzed using FTIR spectroscopy at the Drug Testing Laboratory, Karpagam Academy of Higher Education, Coimbatore. For sample preparation, 2mg of the powdered nanoparticle formulation was blended with 20mg of FTIR-grade KBr and compressed into a pellet. This pellet was then placed in the sample holder and the FTIR spectrum of the polymeric based CUR-NIM loaded nanosuspension was recorded over the range of 4000-500 cm^{-1} at the specified resolution.

Particle size, PDI, Zeta potential analysis

In order to determine the particle size distribution of the polymeric based CUR-NIM loaded nanosuspension, the nanoparticles were analyzed by Dynamic Light Scattering (DLS) using a Malvern Zeta sizer nano range instrument.

***In-vivo* wound healing activity**

Procurement and selection of animals

Healthy Albino Wistar rats of either sex, weighing 150-200g (n = 6), were procured and housed in polypropylene cages with wire-mesh tops under controlled environmental conditions (28 ± 2°C, 12h light/12h dark cycle). Prior to initiating the study, the animals were acclimatized to the laboratory environment for one week. They were

provided with standard pellet feed twice daily and had free access to clean drinking water at all times. Sterilized husk was used as bedding material in the cages and was replaced every three days[36].

Induction of diabetes

Animals from different groups were weighed and their fasting blood glucose levels were measured prior to diabetes induction. Diabetes was experimentally induced through a single intraperitoneal (*i.p.*) administration of freshly prepared Streptozotocin STZ (50mg/kg) dissolved in cold citrate buffer (pH 4.5). To prevent hypoglycemic mortality, the animals were provided with 10% dextrose solution in their drinking water for 48 hours following injection. After five days, fasting blood glucose levels were determined using blood samples collected from the tail vein to confirm diabetic status. Only animals with blood glucose levels exceeding 250mg/dl were selected for the study[36].

Diabetes evaluation

Before and after induction of diabetes, blood glucose level was estimated at specified time intervals such as 3, 5, 7, 12 & 14 days.

Evaluation of wound healing activity

The study animals were allocated into five groups, with each group consisting of six Albino Wistar rats weighing between 150-250g. The details of the group distribution are provided in **(Table 3)**.

Table 3: Experimental protocol

Group No	Group Name	Induction	Treatment	Dose	Route of administration	Grouping
Group I	Control	-	No treatment	-	-	6
Group II	Diabetic control	STZ	-	50mg/kg (STZ, *i.p.*)	Intraperitoneal	6
Group III	Positive control (Standard)	STZ	DPOCL topical solution	50mg/kg (STZ, *i.p.*) + 0.1 ml/cm^2 (≈ 0.232 mg/kg; 0.29 mg/mL solution, Topical DPOCL)	Intraperitoneal + Topical (wound site)	6
Group IV	Test 1	STZ	Polymeric based CUR-NIM loaded nano suspension	50mg/kg (STZ, *i.p.*) + 30mg/kg (Topical Nano suspension)	Intraperitoneal + Topical (wound site)	6
Group V	Test 2	STZ	Polymeric based CUR-NIM loaded nano suspension	50mg/kg (STZ, *i.p.*) + 60mg/kg (Topical Nano suspension)	Intraperitoneal + Topical (wound site)	6

Excision wound model

After injection, wait for one week and the rats were anesthetized with Ketamine HCl administered intraperitoneally at a dose of 80mg/kg body weight. Then, the hairs on the dorsal fur portion were removed using a shaving machine, followed

by depilation and antiseptic treatment. A circular wound area of approximately 300mm² was then created on the dorsal surface using a surgical blade and scissors. The depth of the wound was maintained at 5-7mm with the aid of a biopsy punch. After the procedure, the animals were housed individually in separate cages. The prepared nano formulation was applied topically to the wounds as described and treatment continued until complete healing was observed[37].

Measurement of wound area and contraction

The progression of wound closure was monitored and photographed at specific time points (days 3, 5, 7, 12 and 14) using a digital camera. Wound margins were traced on paper and the corresponding areas were measured with the aid of graph paper. At the conclusion of the experiment, the animals were rehabilitated rather than sacrificed. The percentage of wound contraction was calculated as the reduction in wound size relative to the original area, using the following formula:

$$\text{Percentage wound contraction} = \frac{\text{Initial wound area} - \text{wound area on Nth day}}{\text{Initial wound area}}$$

Statistical analysis

The results were expressed as mean ± SEM and analyzed using one-way ANOVA in IBM SPSS version.25 to evaluate differences between groups. A p-value less than 0.05 was considered statistically significant, whereas values greater than 0.05 were regarded as non-significant.

RESULTS AND DISCUSSION

***In-silico* prediction**

The Lipinski rule of five (Ro5) reveals that the ligand CUR and standard drug DPOCL shows no violations but NIM shows only one violation. CUR and DPOCL scores a better drug-likeness score -0.82 & -0.97 than NIM -0.02. Thus, the violations of these three ligands are within the acceptable limits less than two violations. Hence, the above ligands obey the Lipinski rule of five and it predicts a molecule as suitable for an orally/topically administer drug. Drug-likeness or Ro5 profile of ligands which are listed in **(Table 4)**.

Table 4: Drug-likeness or Lipinski rule of five profile of ligands

Ligand molecules	PubChem CID	Lipinski rule of five						
		M.W.	NHBA	NHBD	LogP	TPSA	No. of violation	Drug-likeness score
		<500 g/mol	<10	<5	<5	<140 Å²	<2	
CUR	969516	368.38	6	2	2.30	93.07	NO (0)	-0.82
NIM	108058	540.61	9	0	3.55	118.3	YES (1)	-0.02
DPOCL (Standard)	135390789	166.90	6	0	1.25	86.75	NO (0)	-0.97

M.W., Molecular Weight; **NHBA**, Number of Hydrogen Bond Acceptor; **NHBD**, Number of ydrogen Bond Donor; **LogP**, Partition coefficient; **TPSA**, Topological Polar Surface Area

ADMET prediction of ligands

Most of the drug candidates under development fail during clinical trials because of unfavourable pharmacokinetic properties and high toxicity. To address this, each molecule was systematically evaluated for its pharmacokinetic profile including absorption, distribution, metabolism, excretion, and toxicity (ADMET) - using the pkCSM predictive tool **(Table 5)**.

Table 5: Absorption, Distribution, Metabolism, Excretion and Toxicity prediction of ligands

Property	Model Name	Predicted Value of ligands		
		CUR	**NIM**	**DPOCL (Standard)**
Absorption	Water solubility **(log mol/L)**	-4.01	-5.754	-0.21
	Caco-2 permeability **(log Papp in 10^{-6} cm/s)**	-0.093	0.922	-0.047
	Intestinal absorption (human) **(% Absorbed)**	82.19	100	56.653
	Skin permeability **(log Kp)**	-2.764	-3.03	-3.309
	P-glycoprotein substrate **(Yes/No)**	Yes	No	No
	P-glycoprotein I inhibitor **(Yes/No)**	Yes	Yes	No
	P-glycoprotein II inhibitor **(Yes/No)**	Yes	Yes	No
Distribution	VDss (human) **(log L/kg)**	-0.215	-0.194	-0.685
	Fraction unbound (human) **(Fu)**	0	0.011	0.939
	BBB permeability **(log BB)**	-0.562	-1.129	-0.811
	CNS permeability **(log PS)**	-2.99	-2.799	-3.28
Metabolism	CYP2D6 substrate **(Yes/No)**	No	No	No
	CYP3A4 substrate **(Yes/No)**	Yes	Yes	No
	CYP1A2 inhibitor **(Yes/No)**	Yes	No	No

	CYP2C19 inhibitor **(Yes/No)**	Yes	No	No
	CYP2C9 inhibitor **(Yes/No)**	Yes	No	No
	CYP2D6 inhibitor **(Yes/No)**	No	No	No
	CYP3A4 inhibitor **(Yes/No)**	Yes	No	No
Excretion	Total clearance **(log ml/min/kg)**	-0.002	0.428	1.156
	Renal OCT2 substrate **(Yes/No)**	No	No	No
Toxicity	AMES toxicity **(Yes/No)**	No	No	No
	Max. tolerated dose (human) **(log mg/ kg/day)**	0.081	-0.371	0.949
	hERG I inhibitor **(Yes/No)**	No	No	No
	hERG II inhibitor **(Yes/No)**	No	No	No
	Oral Rat Acute Toxicity (LD50) **(mol/kg)**	1.833	2.48	2.416
	Oral Rat Chronic Toxicity (LOAEL) **(log mg/kg _bw/day)**	2.228	1.57	0.397
	Hepatotoxicity **(Yes/No)**	No	No	No
	Skin Sensitisation **(Yes/No)**	No	No	No
	T. Pyriformis toxicity **(log ug/L)**	0.494	0.293	-0.048
	Minnow toxicity **(log mM)**	-0.081	1.269	3.544

For orally administration, that CUR and NIM is well suitable that it was confirmed by the following parameters results such as; The water solubility study revealed that the standard drug DPOCL exhibited higher solubility compared to CUR and NIM. The Caco-2 (cell line is composed of human epithelial colorectal adenocarcinoma cells) permeability study revealed that CUR and DPOCL did not exhibit Caco-2 permeability, as their values did not meet the reference threshold of log Papp (10^{-6} cm/s) > 0.90. In contrast, NIM demonstrated Caco-2 permeability with a log Papp value of 0.922 (10^{-6} cm/s), which satisfies the reference criterion. The intestinal absorption study demonstrated that all three compounds (CUR, NIM, and DPOCL) exceeded the reference

absorption threshold of 30%. Notably, the phytoconstituents CUR and NIM exhibited higher absorption rates of 82.19% and 100% respectively, whereas the standard drug DPOCL showed 56.653% absorption. Among these, CUR is predicted to be a substrate of P-glycoprotein (P-gp), an ATP-binding cassette (ABC) transporter while NIM and DPOCL are not considered P-gp substrates. Furthermore, the P-gp inhibition study indicated that all phytoconstituents inhibited P-gp, whereas the standard drug DPOCL did not. The volume of distribution (VDss) study indicated that two phytoconstituents along with the standard drug DPOCL, exhibited low distribution in blood plasma with values falling outside the reference range of 0.71 to 2.81 (log VDss > 0.45). The fraction unbound (Fu) analysis showed that all compounds remained unbound in plasma but comparatively DPOCL demonstrated a higher unbound fraction of 0.237 in human blood which reflecting a greater unbound state to serum proteins compared to CUR and NIM. The blood–brain barrier (BBB) permeability study indicated that all compounds exhibited poor permeability to cross the BBB. Molecules with logBB values greater than 0.3 are considered too readily penetrate the BBB, whereas those with logBB values below −1 are poorly distributed to the brain. In comparison, CUR, NIM, and the standard drug DPOCL showed logBB values of -0.562, -1.129, and -0.811 respectively, confirming their limited BBB permeability as these values fall within the reference range of -1 to 0.3. The Central Nervous System (CNS) permeability study revealed that none of the compounds exhibited significant CNS permeability. Molecules with logPS values greater than -2 are considered capable of crossing the CNS, whereas those with values below -3 are regarded as unable to penetrate. In comparison, CUR and NIM showed logPS values of -2.99 and -2.799 respectively, suggesting borderline permeability while the standard drug DPOCL displayed a logPS value of -3.28 confirming poor CNS permeability within the reference range of -3 to -2.

All the phytoconstituents and the standard drug DPOCL are unlikely to be metabolized as substrates of CYP2D6, an isoform of cytochrome P450 responsible for drug metabolism. In contrast, both the phytoconstituents and DPOCL are likely to undergo metabolism via CYP2D6, ensuring that these compounds do not interfere with drug metabolism. However, one phytoconstituent; CUR appears unlikely to be metabolized by other cytochrome P450 isoforms (CYP1A2, CYP2C19, CYP2C9, CYP3A4). As a result, CUR may influence drug metabolism, unlike NIM and the standard drug DPOCL which do not exhibit such effects. Comparatively, CUR and NIM exhibited notable total clearance values in the range of 0.4 to 1. Among these, CUR demonstrated the lowest clearance value at -0.002, while the standard drug DPOCL showed the highest clearance value of 1.156. Furthermore, CUR, NIM, and DPOCL are unlikely to act as substrates of Organic Cation Transporter 2 (OCT2), which plays a key role in drug disposition and renal clearance. The Maximum Recommended Tolerated Dose (MRTD) was analysed to estimate the toxic dose threshold of chemicals in humans. Based on this assessment, CUR and NIM are considered as having a low MRTD values of 0.081 and -0.371, whereas the standard drug DPOCL exhibited a high MRTD value of 0.949. CUR, NIM, and DPOCL are unlikely to inhibit the hERG I and hERG II genes, which are recognized as key contributors to the development of acquired long QT syndrome and the subsequent risk of fatal ventricular arrhythmia. In addition, these compounds were evaluated for their toxicological parameters including the Lowest Observed Adverse Effect Level (LOAEL) and the No

Observed Adverse Effect Level (NOAEL) and were found not to exhibit hepatotoxicity.

For orally administration, that CUR and NIM is well suitable that it was confirmed by the following parameters results such as; the standard drug DPOCL was predicted to be more aqueous solubility than the CUR and NIM. The skin permeability analysis revealed that all the compounds including standard DPOCL, CUR and NIM have a good skin permeability from the reference value logKp > -2.5. CUR, NIM and DPOCL are considered to be non-mutagenic and therefore not act as a carcinogen. All the compounds were analysed and confirmed to be free from skin sensitization. Even upon direct skin contact, they are unlikely to trigger allergic contact dermatitis which is considered a significant safety concern.

ADMET study display that CUR, NIM has better skin permeability and no skin sensitization. In addition, CUR and NIM shown No Observed Adverse Effect Level. Hence, it can be suitable candidates to formulate topical application. Additionally, the study confirmed that the CUR and NIM are well suitable candidates for orally ingested formulation too, apart from the research related to topical formulation.

Docking interaction analysis

The Phytoconstituents such as CUR, NIM and standard drug DPOCL were docked with the selective targeted proteins which is responsible for wound healing activity such as Interleukins (IL-1, IL-6, IL-20, IL-22, IL-24), matrix metalloproteinase (MMP-8, MMP-9) and tissue inhibitors of metalloproteinases (TIMPs). The binding affinity values reflecting the interactions between ligands and proteins are presented in **(Table 6)** and **(Figure 2)**.

The interaction between CUR and MMP-9 demonstrated that the ligand formed ten Van der Waals contacts with residues ASN A:38, GLU A:47, GLY A:186, MET A:94, PRO A:97, ARG A:98, TYR A:48, TYR A:52, LEU A:187, and ASP A:185. In addition, three conventional hydrogen bonds were observed with ARG A:95, ARG A:51, and THR A:96, while no carbon hydrogen bond interactions were detected, as illustrated in the **(Figure 3)**.

The interaction between CUR and IL-20 demonstrated that the ligand formed seven Van der Waals contacts with residues LEU B:127, SER B:135, HIS B:129, SER B:42, PRO B:130, ASN B:132, and LYS A:121. Additionally, two conventional hydrogen bonds were observed with TYR D:215 and VAL B:43, along with two carbon–hydrogen bond interactions involving GLY D:213 and GLN B:134, as illustrated in the **(Figure 4)**.

The interaction between NIM and MMP-8 demonstrated that the ligand formed seven Van der Waals contacts with residues PHE A:192, SER A:225, ASP A:115, GLU A:118, LEU A:119, LEU A:229, and SER A:228. In addition, two conventional hydrogen bonds were observed with ASN A:226 and TYR A:227, along with a single carbon–hydrogen bond involving THR A:224, as illustrated in the **(Figure 5)**.

The interaction between NIM and IL-20 demonstrated that the ligand formed eleven van der Waals contacts with residues PHE B:131; ASN B:132; GLN B:134; ARG D:214; LEU D:138; PRO B:108; SER D:216; ALA D:217; ARG D:140; HIS B:129; THR D:139. Furthermore, one conventional hydrogen bonds were identified with SER B:135, along with one carbon–hydrogen bond involving PRO B:130, as illustrated in the **(Figure 6)**.

Based on *In-silico* prediction using molecular docking results, CUR and NIM have shown significant binding energy than the standard drug DPOCL. CUR scored highest binding energy with four proteins i.e., MMP-9 (-8.4 Kcal/mol), IL-20 (-7.6 Kcal/mol), IL-22 (-7.4 Kcal/mol) and MMP-

8 (-7.1 Kcal/mol). NIM scored highest binding energy with three proteins i.e., MMP-8 (-8.5 Kcal/mol), IL-20 (-7.7 Kcal/mol) and IL-22 (-6.6 Kcal/mol). Among those, CUR has shown significant binding affinity with MMP-9, IL-20 and NIM has shown significant binding affinity with MMP-8, IL-20 which are well responsible for wound healing activity.

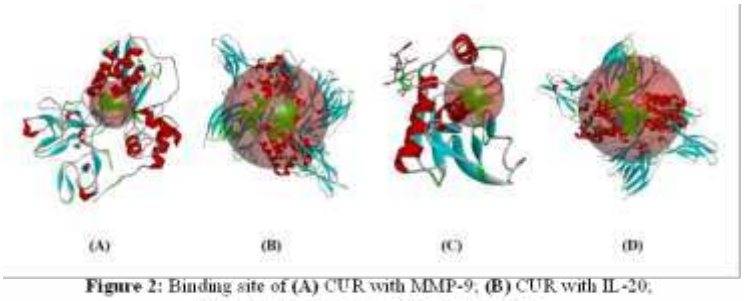

Figure 2: Binding site of **(A)** CUR with MMP-9; **(B)** CUR with IL-20; **(C)** NIM with MMP-8; **(D)** NIM with IL-20

Table 6: Binding energy of ligand-protein interaction

S.no	Targets (Proteins)	Binding energy of ligand-protein interaction (Kcal/mol)		
		CUR	NIM	DPOCL (Standard)
1.	Interleukin-1 (IL-1)	-6.7	-6.4	-4.1
2.	Interleukin-6 (IL-6)	-5.7	-6.2	-4.4
3.	Interleukin-20 (IL-20)	-7.6	-7.7	-5.3
4.	Interleukin-22 (IL-22)	-7.4	-6.6	-4.7
5.	Interleukin-24 (IL-24)	-6.0	-5.6	-4.7
6.	Matrix metalloproteinase-8 (MMP-8)	-7.1	-8.5	-5.0
7.	Matrix metalloproteinase-9 (MMP-9)	-8.4	-6.2	-5.1
8.	Tissue inhibitors of metalloproteinase (TIMP)	-6.7	-6.4	-4.4

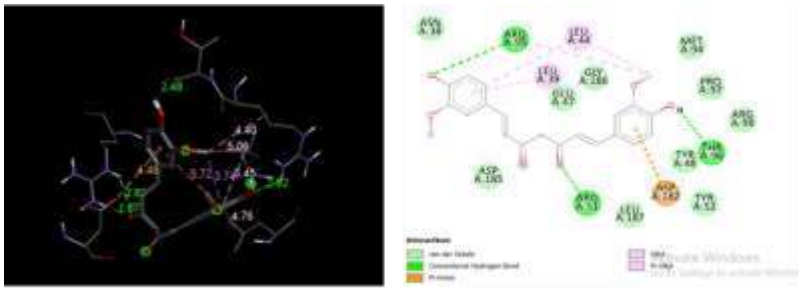

Figure 3: 3D and 2D complex of Curcumin and MMP-9

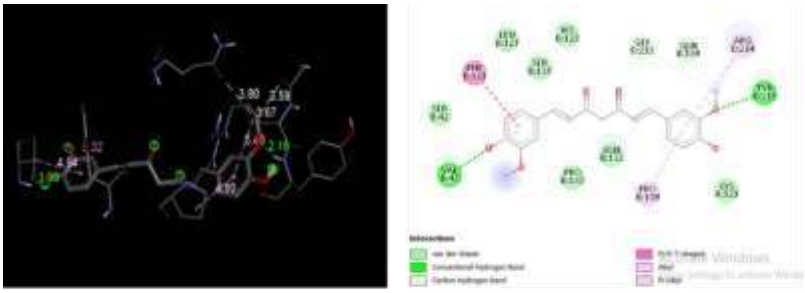

Figure 4: 3D and 2D complex of Curcumin and IL-20

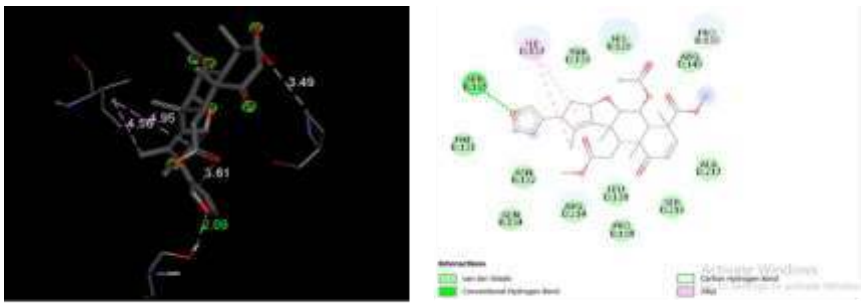

Figure 6: 3D and 2D complex of Nimbin and IL-20

Phytochemical screening of neem seed extract and NIM

The percentage yield of the methanolic extract of Azadirachta indica (semisolid dark brownish color) was 48.27%, indicating a high efficiency of extraction, which is acceptable and within the expected range for methanolic extraction of phytochemicals from plant materials. The methanolic extract of Azadirachta indica followed by isolation of NIM was subjected to phytochemical screening for various chemical tests as per the standard reported methods and was found to contain alkaloids, flavonoids, saponins, glycosides, terpenoids, polyphenols and tannins, steroids, coumarins that are useful for healing of wounds **(Table 7) (Figure 7)**. Based on that result, the neem seed extract shows that the presence of alkaloids, flavonoids, saponins, terpenoids but the isolated compound has shown only the presence of terpenoids. Thus, it confirms that the isolated compound is NIM because NIM is a limonoids class of triterpenoid which may possess the wound healing activity.

Table 7: Preliminary Phytochemical Evaluation

S. No.	Phytochemicals	Name of test	NSE Result	NIM Result
1.	Alkaloids	Mayer's test	-	-
		Wagner's test	++	-
2.	Flavonoids	Alkaline reagent test	+	-
		Shinoda test	-	-
3.	Saponins	Foam test	+	-
4.	Glycosides	Salkowski's test	-	-
		Keller- kiliani test	-	-
5.	Terpenoids	Terpenoids test	+++	+++
6.	Polyphenols and tannins	Polyphenols and tannins	-	-
7.	Steroids	Steroids test	-	-
8.	Coumarins	Coumarins test	-	-

NSE, Neem Seed Extract; **NIM**, Nimbin; **(+)** In traces; **(++)** Present in moderate amount; **(+++)** More amount is present

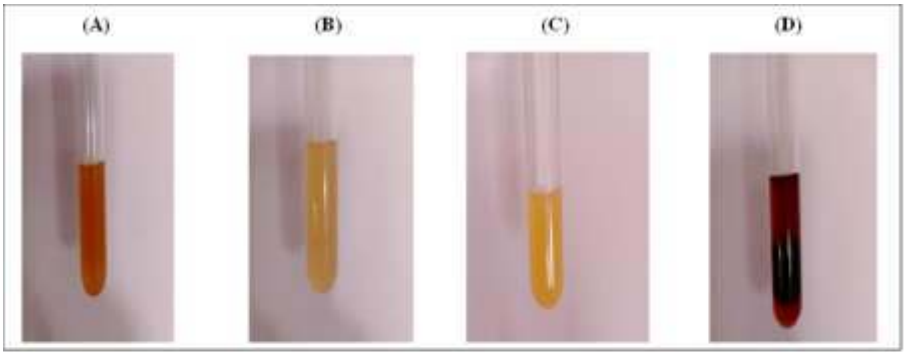

Figure 7: Phytochemical Evaluation,
(A) Test for Alkaloids, (B) Test for Flavonoids, (C) Test for Saponins, (D) Test for Terpenoids

Fabrication & Characterization of Polymeric based CUR-NIM loaded nanosuspension

Visual examination

After adding the CUR and NIM mixed organic phase with the aqueous phase containing SLS & β-CD, rapid miscibility of methanol with water was observed. This increased the polarity of methanol and reduced the solubility of CUR and NIM, initiating crystal nucleation that it looks like yellowish precipitate solution prior to sonication. The process of sonication subsequently removed residual methanol from the nanosuspension and facilitating the formation of CUR nanocrystals that complexed with β-CD. Then resulting suspension was then subjected to centrifugation to separate the SLS/β-CD mixed CUR-NIM nanoparticles, which were re-dispersed in distilled water to yield a polymeric CUR-NIM nanosuspension.

UV-Visible Analysis

UV-Visible spectroscopy was used for preliminary confirmation of formation of polymeric based CUR-NIM loaded nanoparticles in nanosuspension with their surface plasmon resonance (SPR peak). The reaction time was evaluated using time-dependent UV-Visible spectroscopy. The analysis revealed that nanoparticle formation commenced immediately after the reaction, as evidenced by the appearance of SPR bands around 429nm at room temperature **(Figure 8)**. A notable shift in the absorption peak was recorded, moving from 270nm to 430nm. With increasing reaction time (0 to 2h), a progressive rise in the SPR peak confirmed the formation of polymeric based CUR-NIM loaded nanoparticles. Moreover, the gradual narrowing of the peaks over time indicated the monodispersity of the particles.

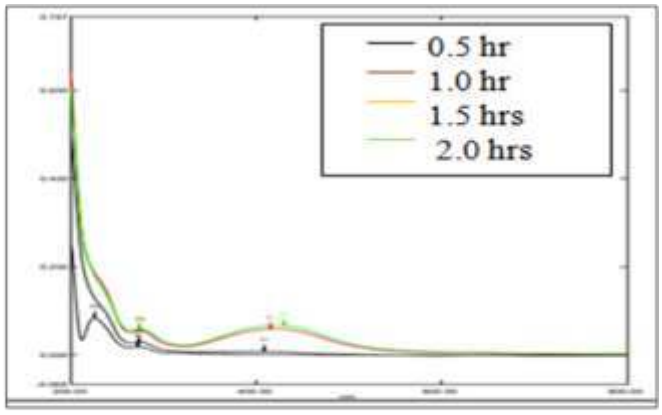

Figure 8: Time dependent UV-Visible absorbance spectra by UV for Polymeric based CUR-NIM loaded nanosuspension

FTIR analysis

The functional groups present in pure CUR, isolated NIM from neem seed kernel, and the polymeric based CUR-NIM loaded nanosuspension were characterized using FTIR spectroscopy **(Table 8)**. The spectra provided insights into the surface chemistry of CUR and NIM. The observed peaks confirmed the presence of characteristic groups such as C=O, C–O, C–H, and O–H which played key roles in capping, reduction and stabilization of the polymeric based CUR-NIM loaded nanosuspension.

The FTIR spectrum of the pure sample of CUR, the peaks are observed at 3506.46 cm^{-1} (Broad phenolic –OH stretching), 1626.57 cm^{-1} (C=O group in conjugated system), 1601.18 cm^{-1} (Aromatic C=C stretching), 1505.79 cm^{-1} (C=C stretching in ring; Good aromatic skeletal vibrations), 1427.38 cm^{-1} (C–C Stretching or CH_2 bending), 1315.42 cm^{-1} to 1025.30 cm^{-1} (C–O stretching of phenolic/methoxy), 977.65 cm^{-1} (=C–H out-of-plane bending from trans-alkene in the conjugated chain), 961.68 cm^{-1} (=C–H wagging (trans-alkene or conjugated enone system), 885.37 cm^{-1} (Aromatic C–H out-of-plane bend (meta-substituted phenyl ring)), 855.77 cm^{-1} (Aromatic ring deformation or CH_2 rocking can come from the aromatic ring with –OH or $–OCH_3$), 807.70 cm^{-1} (Aromatic C–H out-of-plane bending (ortho-substituted phenyl ring)) & 714.16 cm^{-1} (Aromatic ring deformation (mono- or para-substituted, possibly ring puckering vibrations)). Additional peaks observed in the region below 1000 cm^{-1} (977.65 to 714.16 cm^{-1}) correspond to aromatic C–H out-of-plane bending vibrations and trans-alkene groups, further supporting the structural features of curcumin **(Figure 9)**.

The sample of NIM peaks are observed at 3327.00 cm^{-1} (Broad –OH stretching from lactone ring or hemiacetal), 2939.72 cm^{-1} (C–H stretching represent aliphatic $–CH_2$ and $–CH_3$ groups), 2832.31 cm^{-1} (C–H stretching which represent multiple methoxy ($O–CH_3$) groups present), 1603.97 cm^{-1} (C=C or C=O stretching (possibly from aromatic ring or conjugated)), peaks at 1399.09 cm^{-1} and 1020.28 cm^{-1} are attributed to C–H deformation and C–O stretching, confirming the presence of ester and ether groups **(Figure 10)**.

After incorporation of CUR and NIM with suitable polymers, the polymeric based CUR-NIM loaded nanosuspension exhibited absorption bands corresponding to characteristic functional groups. Broad O–H, C=O, and C–O stretching vibrations were observed in the IR spectrum at 3283.60 cm^{-1}, 1639.52 cm^{-1}, and 1015.67 cm^{-1} respectively, confirming their presence in the prepared nano formulation and indicating structural stability **(Figure 11)**. These findings suggest that carbonyl compounds, hydroxyl groups and ketone functionalities played a pivotal role in nanoparticle formation and stabilization by facilitating capping, reduction and stabilizing interactions during the synthesis of the polymer-based CUR-NIM loaded nanosuspension. Because, carbonyl and ketone groups are providing polar sites for interaction with polymer matrices or drug molecules, aiding in encapsulation and surface chemistry. Hydroxyl groups are actively participated in hydrogen bonding, thereby enhance solubility and stabilize the nanosuspension by preventing agglomeration.

Table 8: FTIR vibrational frequencies and its functional groups

S. No	Sample	Vibrational frequencies (cm^{-1})	Functional groups
1.	CURCUMIN (CUR)	3506.46	O-H
		1626.57	C=O
		1601.18	C=C
		1505.79	C=C
		1427.38	C-C or CH_2
		1315.42	C-O
		1273.17	C-O
		1231.99	C-O
		1203.98	C-O
		1181.75	C-O
		1151.40	C-O
		1114.14	C-O
		1025.30	C-O
2.	NIMBIN (NIM)	3327.00	O-H
		2939.72	C-H
		2832.31	C-H
		1603.97	C=C or C=O
		1399.09	C-H
		1020.28	C-O
3.	Polymeric based CUR-NIM loaded nanosuspension	3283.60	O-H
		1639.52	C=O
		1015.67	C-O

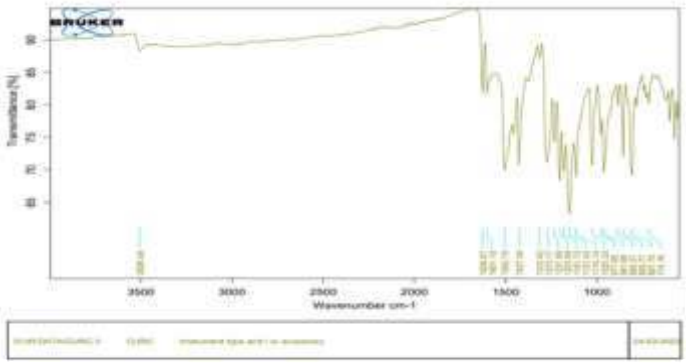

Figure 9: FTIR spectrum of Curcumin

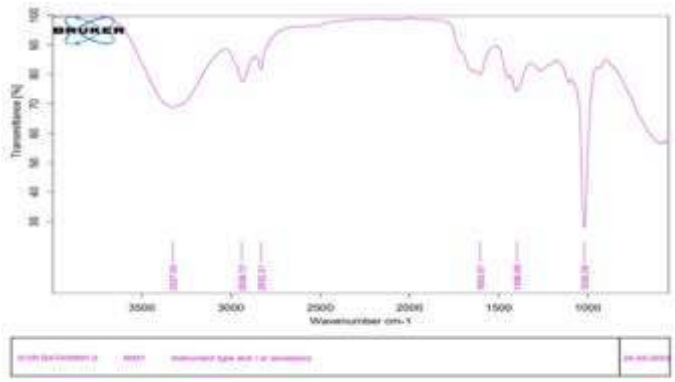

Figure 10: FTIR spectrum of Nimbin

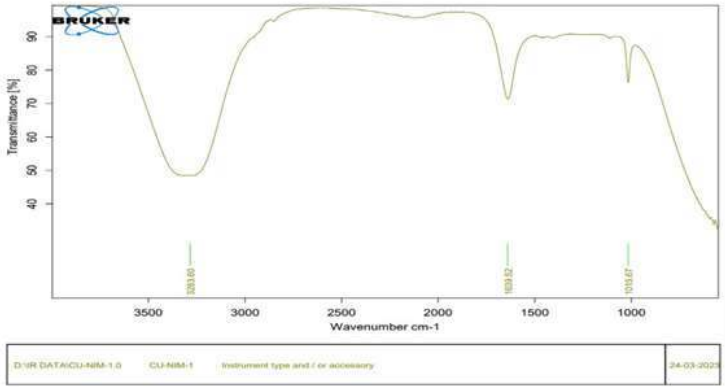

Figure 11: FTIR spectrum of Polymeric based CUR-NIM loaded nanosuspension

Particle size, PDI, Zeta potential analysis

Particle size analysis using dynamic light scattering (DLS) revealed that the synthesized polymeric based CUR-NIM loaded nanoparticles had a size distribution ranging from 370 to 385.6nm. The Z-average particle size and highest intensity peak of the CUR-NIM loaded nano formulation denotes that the particles were more distributed at 380.6nm, indicating that the majority of particles contributed significantly to light scattering intensity at this size. However, the primary size population observed in the volume distribution was centered around 100nm, indicating the presence of smaller nanoparticles as the major component by volume. For topical delivery, even up to 500nm is fine. That confirms it can penetrate damaged or inflamed skin as in DFU, so 380.6nm is suitable. The polydispersity index (PDI) value was 0.5421 with intercept 0.8882, suggesting a moderate degree of size heterogeneity. Even though this value exceeds the commonly preferred threshold for monodisperse systems, it remains acceptable for topical applications. Because, where a broader size distribution can still ensure effective skin penetration. Additionally, Zeta Potential of prepared polymeric based CUR-NIM loaded nanoparticles was -26 mv indicated moderate stability and no signs of aggregation, acceptable for formulation purposes. This study result reveals that Anion present in nano formulation could be more stable, permeable and interact favourably with cell membranes because all the cell membrane are negatively charged. A graphical representation of particle size, polydispersity index, and zeta potential of the polymeric based CUR-NIM loaded nanosuspension is presented in the **(Figure 12 & 13)**.

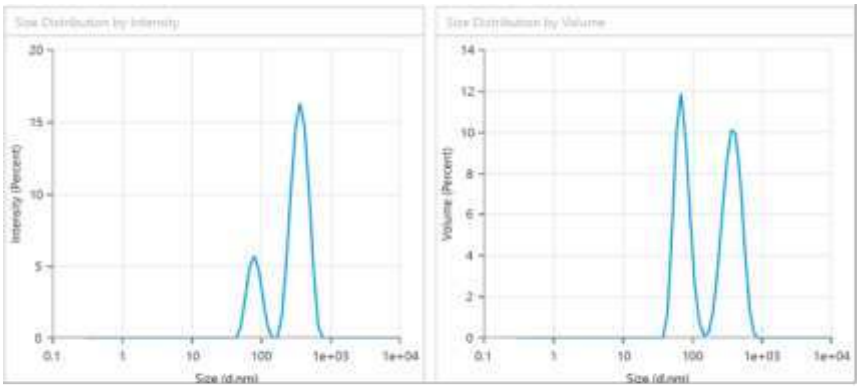

Figure 12: Particle size distribution of synthesized polymeric based CUR-NIM loaded nanoparticles by DLS based on intensity

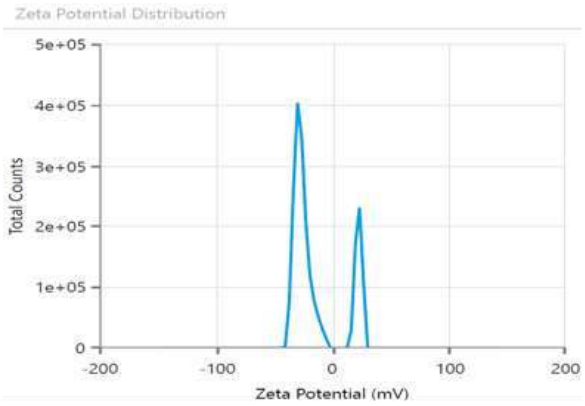

Figure 13: Average Zeta Potential: -26 mv

***In-vivo* wound healing activity**

Before induction of diabetes i.e., at 0th day fasting blood glucose level of all groups was found to be normal. At 7th day observation, blood glucose level was increased and at 14th day, slightly it has been reduced **(Table 9)**.

Table 9: Monitoring of fasting blood glucose level

Groups	Fasting blood glucose level (mg/dl) before induction 0 day	Fasting blood glucose level (mg/dl) after induction	
		7th day	14th day
Control	125 ± 0.45	296 ± 0.53	196 ± 0.34
Diabetic control	137 ± 0.34	274 ± 0.52	184 ± 0.46
Standard Positive control (DPOCL)	126 ± 0. 51	287 ± 0.47	170 ± 0.42
Test 1 (CUR-NIM 30mg/kg)	138 ± 0. 72	290 ± 0.33	177 ± 0.25
Test 2 (CUR-NIM 60mg/kg)	124 ± 0.43	301 ± 0.46	165 ±0.38

The wound healing efficacy of the prepared polymeric based CUR-NIM loaded nanosuspension was evaluated in adult Albino Wistar rats by measuring the percentage of wound contraction. The results are summarized in **(Table 10)**, and the experimental animals are depicted in the **(Figure 14)**. The wound area (mm^2) in each animal group was measured on the 3rd, 5th, 7th, 12th and 14th days. This study included a control group, a diabetes-induced group, a standard treatment group, Test 1 (polymeric based CUR-NIM loaded nanosuspension administered to rats with 30mg/kg STZ-induced diabetes), and Test 2 (polymeric based CUR-NIM loaded nanosuspension administered to rats with 60mg/kg STZ-induced diabetes). On the 14th day, wound healing was compared across five groups. The polymeric based CUR–NIM loaded nanosuspension exhibited nearly equivalent diabetic wound healing activity comparable to standard drug DPOCL topical solution and higher than the other groups of rats.

Table 10: Percentage rate of wound contraction in rats

Groups	% Wound contraction in different days in sq.mm				
	3rd day	5th day	7th day	12th day	14th day
Control	36.32 ± 1.06	43.21 ± 1.22	58.16 ± 2.12	69.99 ± 2.24	77.14 ± 3.62
Diabetic control	21.02 ± 2.10	39.32 ± 2.01	50.40 ± 1.87	62.33 ± 2.10	68.57 ± 1.32
Standard Positive control (DPOCL)	63.13 ± 1.33	79.87 ± 2.26	91.73 ± 3.13	96.67 ± 2.54	100 ± 2.37
Test 1 (CUR-NIM 30mg/kg)	51.88 ± 1.49	60.46 ± 1.12	69.7 ± 2.13	80.56 ± 1.66	87.81 ± 2.63
Test 2 (CUR-NIM 60mg/kg)	65.20 ± 2.87	70.33 ± 3.44	81.14 ± 2.95	89.89 ± 2.28	97.12 ± 3.45

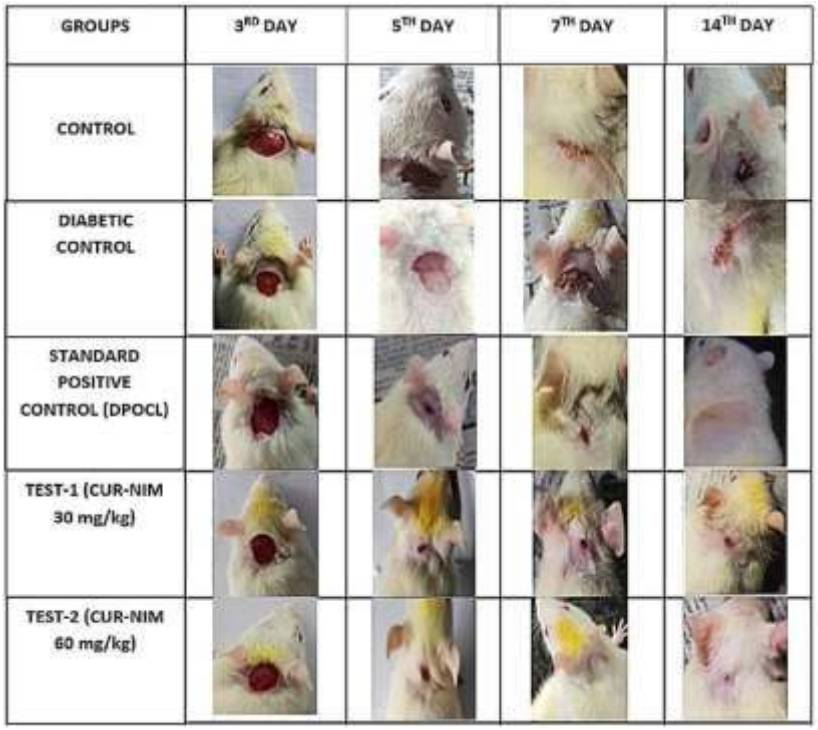

Figure 14: Wound healing observation in rats

All the five groups showed decreasing wound area from day to day. On 14th day, Group-I (control) exhibit 77.14% wound contraction which may be due to self-immunity of animals, Group-II (diabetes induced control) showed 68.57% wound contraction (the healing rate was low due to diabetes which impaired the wound healing effect), Group-IV (Polymeric based CUR-NIM loaded nanosuspension, 30mg/kg) and Group-V (Polymeric based CUR-NIM loaded nanosuspension, 60mg/kg) exhibits 87.81% and 97.12% wound contraction respectively. Group-III (Standard Positive Control - Diperoxochloric acid topical solution) shown 100% wound contraction, it exhibits complete wound healing by 14th day indicates rapid epithelization and collagenization.

Hence, the animals treated with topically applied Polymeric based CUR-NIM loaded nanosuspension (CUR-NIM 60 mg/kg) has shown almost equivalent diabetic wound healing and epithelization activity as compared with the positive control group.

On performing one-way ANOVA for the wound healing activity between the group effect has a p-value of 0.006085 which is less than 0.05. Therefore, the result is significant. From the Tukey test for two-way ANOVA, the p-value obtained for CUR-NIM 60mg/kg and diabetic control is 0.032, since it is less than 0.05, we conclude that the result is statistically significant. The p-value obtained for standard drug and diabetic control is 0.010, since it is less than 0.05, we conclude that the result is statistically significant **(Figure 15)**.

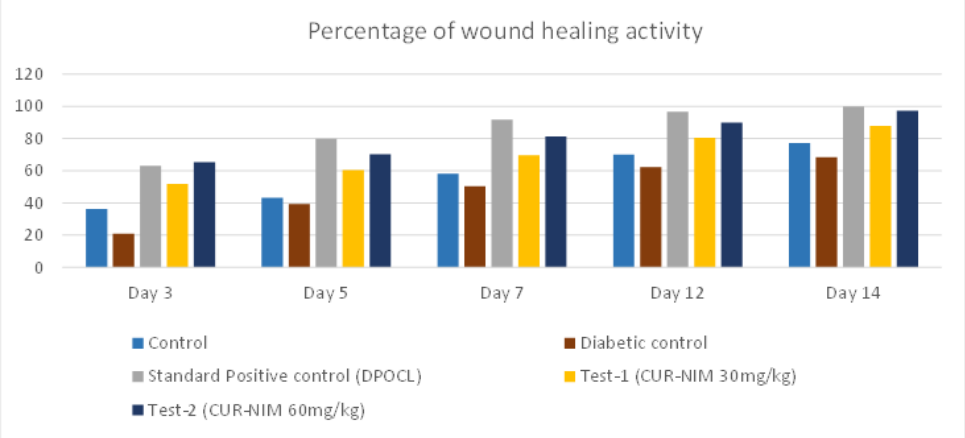

Figure 15: Percentage of wound healing activity

CONCLUSION

From this study, it can be concluded that the polymeric based CUR-NIM loaded nanosuspension exhibited significantly good wound healing activity for diabetic foot ulcer. *In-silico* studies confirmed that the CUR shows significant binding affinity with MMP-9, IL-20 and NIM shows significant binding affinity with MMP-8, IL-20 which are well responsible for wound healing activity comparatively standard drug DPOCL. The enhanced potency of the polymer-based CUR-NIM nanosuspension can be attributed to particle size reduction, which enhanced aqueous solubility and permeability, while also increasing the reactivity of CUR through its incorporation with NIM using β-cyclodextrin (β-CD) as the polymer and sodium lauryl sulphate (SLS) as the surfactant. Because, the NIM is a promising candidate to promote the wound healing and also acts as a synergistic molecule to enhance the activity of CUR to treat the DFU. Further lot of *In-vitro* and *In-vivo* molecular & mechanistic studies require for confirm the clinical usage of this Polymeric based CUR-NIM loaded nanosuspension.

ACKNOWLEDGEMENTS

The authors are gratefully express thanks for the facilities provided by Managing Trustee of Karpagam Charity Trust, Karpagam Academy of Higher Education and Karpagam College of Pharmacy, Coimbatore, Tamil Nadu, India.

Author contribution

G.P.V., and S.K.C. designed the study; G.P.V., N.J., M.N.M., E.M. performed the research including *in silico* studies, purchasing curcumin, isolation & phytochemical screening of Nimbin, fabrication of nanoformulation and *in vivo* studies; S.K.C., and M.S. provided resources and supervised the study; G.P.V., and S.K.C.

characterized the nanoparticles and nanoformulation; G.P.V., S.K.C., N.J., M.N.M., E.M., and M.S. analyzed the data; G.P.V., wrote the manuscript. All authors reviewed the manuscript.

Relevant conflicts of interest/financial disclosures: The authors declare that the research was conducted in the absence of any commercial or financial relationships that could be construed as a potential conflict of interest.

Compliance with Ethical Standards This article does not contain any studies with human participants performed by any of the authors.

Consent for publication All authors agree to submit the research article to the journal and accept complete responsibility for the contents of the article.

Ethics approval Applicable (The animal experimental protocols were approved by Institutional Animal Ethics Committee (IAEC) of Karpagam Academy of Higher Education (KAHE), Coimbatore, Tamil Nadu under approval number KAHE/IAEC/2023/04-02/014, following CPCSEA guidelines).

REFERENCES

1. Armstrong DG, Boulton AJM, Bus SA. Diabetic Foot Ulcers and Their Recurrence. N Engl J Med. 2017 Jun 15 [cited 2026 Jan 4];376(24):2367–75.
2. Zhang P, Lu J, Jing Y, Tang S, Zhu D, Bi Y. Global epidemiology of diabetic foot ulceration: a systematic review and meta-analysis †. Ann Med. 2017 Feb 17 [cited 2026 Jan 4];49(2):106–16.
3. Ezhilarasu H, Vishalli D, Dheen ST, Bay BH, Kumar Srinivasan D. Nanoparticle-Based Therapeutic Approach for Diabetic Wound Healing. Nanomaterials. 2020 Jun 1 [cited 2026 Jan 4];10(6):1234.
4. Syafril S. Pathophysiology diabetic foot ulcer. IOP Conf Ser Earth Environ Sci. 2018 Mar 26;125(1).
5. Zhang Y, van Netten JJ, Baba M, Cheng Q, Pacella R, McPhail SM, et al. Diabetes-related foot disease in Australia: a systematic review of the prevalence and incidence of risk factors, disease and amputation in Australian populations. J Foot Ankle Res. 2021 Dec 1 [cited 2026 Jan 4];14(1):8.
6. L Y, M N, S A. Literature review on the management of diabetic foot ulcer. World J Diabetes. 2015 [cited 2026 Jan 4];6(1):37.
7. Kavitha KV, Tiwari S, Purandare VB, Khedkar S, Bhosale SS, Unnikrishnan AG. Choice of wound care in diabetic foot ulcer: A practical approach. World J Diabetes. 2014 [cited 2026 Jan 4];5(4):546.
8. Bowlby M, Blume P, Schmidt B, Donegan R. Safety and efficacy of Becaplermin gel in the treatment of diabetic foot ulcers. Chronic Wound Care Manag Res. 2014 Jul [cited 2026 Jan 4];11.
9. Raju R, Kethavath SN, Sangavarapu SM, Kanjarla P. Efficacy of Cadexomer Iodine in the Treatment of Chronic Ulcers: A Randomized, Multicenter, Controlled Trial. Wounds (King Prussia, Pa). 2019;
10. Dumville JC, Lipsky BA, Hoey C, Cruciani M, Fiscon M, Xia J. Topical antimicrobial agents for treating foot ulcers in people with diabetes. Cochrane database Syst Rev. 2017 Jun 14 [cited 2026 Jan 4];6(6).
11. Porwal S, Malviya R, Sundram S, Sridhar SB, Shareef J. Diabetic Wound Healing: Factors, Mechanisms, and Treatment Strategies Using Herbal Components. Curr Drug Targets. 2025 Jan 10 [cited 2026 Jan 4];26(6):367–81.
12. Chumpolphant S, Suwatronnakorn M, Issaravanich S, Tencomnao T, Prasansuklab

A. Polyherbal formulation exerts wound healing, anti-inflammatory, angiogenic and antimicrobial properties: Potential role in the treatment of diabetic foot ulcers. Saudi J Biol Sci. 2022 Jul 1 [cited 2026 Jan 4];29(7):103330.

13. Kesharwani P, Jain A, Srivastava AK, Keshari MK. Systematic development and characterization of curcumin-loaded nanogel for topical application. Drug Dev Ind Pharm. 2020 [cited 2026 Jan 4];46(9):1443–57.
14. Alven S, Nqoro X, Aderibigbe BA. Polymer-Based Materials Loaded with Curcumin for Wound Healing Applications. Polymers (Basel). 2020 Oct 1 [cited 2026 Jan 4];12(10):1–25.
15. Moorthi C, Krishnan K, Manavalan R, Kathiresan K. Preparation and characterization of curcumin-piperine dual drug loaded nanoparticles. Asian Pac J Trop Biomed. 2012 [cited 2026 Jan 4];2(11):841.
16. Moorthi C, Senthil Kumar C, Mohan S, Kathiresan K. SLS/βCD-curcumin nanosuspension: Preparation, characterization and pharmacological evaluation. J Pharm Res. 2013 Mar [cited 2026 Jan 4];7(3):219–23.
17. Kiti K, Suwantong O. Bilayer wound dressing based on sodium alginate incorporated with curcumin-β-cyclodextrin inclusion complex/chitosan hydrogel. Int J Biol Macromol. 2020 Dec 1 [cited 2026 Jan 4];164:4113–24.
18. Gomez C, Muangnoi C, Sorasitthiyanukarn FN, Wongpiyabovorn J, Rojsitthisak P, Rojsitthisak P. Synergistic Effects of Photo-Irradiation and Curcumin-Chitosan/Alginate Nanoparticles on Tumor Necrosis Factor-Alpha-Induced Psoriasis-Like Proliferation of Keratinocytes. Molecules. 2019 Apr 9 [cited 2026 Jan 4];24(7).
19. Akbar MU, Zia KM, Akash MSH, Nazir A, Zuber M, Ibrahim M. In-vivo anti-diabetic and wound healing potential of chitosan/alginate/maltodextrin/pluronic-based mixed polymeric micelles: Curcumin therapeutic potential. Int J Biol Macromol. 2018 Dec 1 [cited 2026 Jan 4];120:2418–30.
20. Khanal P, Mandar BK, Patil BM, Hullatti KK. In silico Antidiabetic Screening of Borapetoside C, Cordifolioside A and Magnoflorine. Indian J Pharm Sci. 2019 Jun 27 [cited 2026 Jan 4];81(3):550–5.
21. Lipinski CA, Lombardo F, Dominy BW, Feeney PJ. Experimental and computational approaches to estimate solubility and permeability in drug discovery and development settings. Adv Drug Deliv Rev. 2001 Mar 1 [cited 2026 Jan 4];46(1–3):3–26.
22. Kuppusamy A, Arumugam M, George S. Combining in silico and in vitro approaches to evaluate the acetylcholinesterase inhibitory profile of some commercially available flavonoids in the management of Alzheimer's disease. Int J Biol Macromol. 2017 Feb 1 [cited 2026 Jan 4];95:199–203.
23. Wang Y, Shao T, Wang J, Huang X, Deng X, Cao Y, et al. An update on potential biomarkers for diagnosing diabetic foot ulcer at early stage. Biomed Pharmacother. 2021 Jan 1 [cited 2026 Jan 4];133.
24. Pichu S, Patel BM, Apparsundaram S, Goyal RK. Role of biomarkers in predicting diabetes complications with special reference to diabetic foot ulcers. Biomark Med. 2017 Apr 1 [cited 2026 Jan 4];11(4):377–88.
25. Mun CS, Hui LY, Sing LC, Karunakaran R, Ravichandran V. Multi-targeted molecular docking, pharmacokinetics, and drug-likeness evaluation of coumarin based compounds targeting proteins involved in development of COVID-19. Saudi J Biol Sci. 2022 Dec 1;29(12).
26. Cheng F, Li W, Zhou Y, Shen J, Wu Z, Liu G, et al. admetSAR: a comprehensive source and

free tool for assessment of chemical ADMET properties. J Chem Inf Model. 2012 Nov 26 [cited 2026 Jan 4];52(11):3099–105.
27. Trott O, Olson AJ. AutoDock Vina: improving the speed and accuracy of docking with a new scoring function, efficient optimization and multithreading. J Comput Chem. 2010 Jan 30 [cited 2026 Jan 4];31(2):455.
28. Sudhakaran G, Prathap P, Guru A, Rajesh R, Sathish S, Madhavan T, et al. Anti-inflammatory role demonstrated both in vitro and in vivo models using nonsteroidal tetranortriterpenoid, Nimbin (N1) and its analogs (N2 and N3) that alleviate the domestication of alternative medicine. Cell Biol Int. 2022 May 1 [cited 2026 Jan 4];46(5):771–91.
29. Khanal S. Qualitative and Quantitative Phytochemical Screening of Azadirachta indica Juss. Plant Parts. Int J Appl Sci Biotechnol. 2021 Jun 28;9(2):122–7.
30. sahrawat A, Sharma J, Rahul SN, Tiwari S, Joshi MD, Pundhir A, et al. Phytochemical analysis and Antibacterial properties of Azadirachta indica (Neem) leaves extract against E.coli. J Pharmacogn Phytochem. 2018 Jul 25 [cited 2026 Jan 4];7(4):1368–71.
31. S. G, SENTHILRAJ R, A. TB, S. S, M. TK. PHYTOCHEMICAL SCREENING AND ANTIMICROBIAL ACTIVITY OF AZADIRACHTA INDICA AND PLECTRANTHUS AMBOINICUS EXTRACT. Int J Curr Pharm Res. 2020 Jan 10 [cited 2026 Jan 4];14–7.
32. Chidambaram M, Chinnamaruthu S, Sellappan M, Krishnasamy K. Anionic Surfactant Based Topical Curcumin Nanosuspension: Fabrication, Characterization and Evaluation. Nano Biomed Eng. 2013 May 28;5(2).
33. Pınar SG, Canpınar H, Tan Ç, Çelebi N. A new nanosuspension prepared with wet milling method for oral delivery of highly variable drug Cyclosporine A: development, optimization and in vivo evaluation. Eur J Pharm Sci. 2022 Apr 1 [cited 2026 Jan 4];171.
34. Liu X, Gan H, Hu C, Sun W, Zhu X, Meng Z, et al. Silver sulfadiazine nanosuspension-loaded thermosensitive hydrogel as a topical antibacterial agent. Int J Nanomedicine. 2018 [cited 2026 Jan 4];14:289–300.
35. Madeswaran A, Tamilazhagan S, Mohan S. In silico evaluation, characterization, and in vitro anticancer activity of curcumin–nimbin loaded nanoformulation in HCT-116 cell lines. Biotechnologia. 2024 [cited 2026 Jan 4];105(4):355–65.
36. El-Naggar ME, Al-Joufi F, Anwar M, Attia MF, El-Bana MA. Curcumin-loaded PLA-PEG copolymer nanoparticles for treatment of liver inflammation in streptozotocin-induced diabetic rats. Colloids Surf B Biointerfaces. 2019 May 1 [cited 2026 Jan 4];177:389–98.
37. de Moura Estevão LR, Cassini-Vieira P, Leite AGB, de Carvalho Bulhões AAV, da Silva Barcelos L, Evêncio-Neto J. Morphological Evaluation of Wound Healing Events in the Excisional Wound Healing Model in Rats. Bio-protocol. 2019 Jul 5 [cited 2026 Jan 4];9(13):e3285.

HOW TO CITE: Gnana Prakash Victor, Senthil Kumar Chinnamaruthu, Nithyasri Jayavel, Mohamed Nizar Mustafa, Eraiarasu Mahadevan, Mohan Sellappan, In-silico Prediction, Fabrication, Characterization and Wound Healing Activity of Polymeric Based Curcumin-Nimbin Loaded Nanosuspension for Diabetic Foot Ulcer Using Diabetogenic Induced Rat Models, Int. J. of Pharm. Sci., 2026, Vol 4, Issue 6, 7646-7671, https://doi.org/10.5281/zenodo.21066238